Thin Solid Films 632 (2017) 17–22

Contents lists available at ScienceDirect

Thin Solid Films

journal homepage: www.elsevier.com/locate/tsf

The influence of surface oxides on the mechanical response of oxidized grain boundaries

Judith Dohr [a,*], David E.J. Armstrong [a], Edmund Tarleton [a], Thierry Couvant [b], Sergio Lozano-Perez [a]

[a] Department of Materials Science, University of Oxford, Parks Road, Oxford OX1 3PH, UK
[b] EDF R&D, Avenue des Renardières, 77818 Moret-sur-Loing cedex, France

ARTICLE INFO

Article history:
Received 13 September 2016
Received in revised form 30 March 2017
Accepted 30 March 2017
Available online 31 March 2017

Keywords:
Nickel alloys
Oxidation
Grain boundary embrittlement
Stress corrosion cracking
Mechanical properties testing
Micromechanical modeling
Micromechanical testing
Corrosion

ABSTRACT

The mechanical response of oxidized grain boundaries in a nickel alloy used for nuclear applications has been investigated by performing microcantilever bend tests. It was found that whilst failure can proceed along the oxide-metal interface not all oxidized grain boundaries exhibit intergranular failure. The presence of an external surface oxide has been identified as playing a crucial role in influencing the mechanical response. By removing the surface oxide, using a focused ion beam, tests were performed on the same grain boundaries with and without a surface oxide layer, and showed that surface oxides can suppress or delay fracture. Taking into account the effect of the surface oxide on microcantilever tests, it was possible to present the most accurate parameterization of the local stress at failure of oxidized grain boundaries to date and to predict the experimentally observed behavior via realistic cohesive damage finite element simulations, which further underline the experimental observations.

1. Introduction

Microscopic events are often at the root of the macroscopic material response. Material failure due to stress corrosion cracking (SCC), which is a localized sub-mode of corrosion that manifests itself on the micro-scale, is no exception. Even though many SCC mechanisms have been proposed and widely discussed [1–4], in-depth understanding of the crack initiation and propagation and the role of local microstructure is still lacking. Realistic predictions of SCC in austenitic alloys, such as Alloy 600, widely used in pressurized water reactor (PWR) primary coolant environments, via large-scale engineering models is a priority to the nuclear industry. This includes an accurate parameterization of multiple influencing factors (typically crystallographic, environmental and mechanical). In particular, the modeling of local behaviors at grain boundaries may help to significantly improve predictive models [5] of component degradation and lifetime. However, success strongly depends upon a better understanding of the underlying mechanisms that control the failure and, as identified by Couvant et al. [5], the determination of the failure stress of oxidized grain boundaries is a particular challenge, not least because of the limited penetration depths of intergranular (IG) oxidation — which precludes the use of traditional mechanical testing methods. As demonstrated by Fujii et al. [6], Dugdale et al. [7] and Stratulat et al. [8], micromechanical tests are a powerful tool for studying the mechanical response of single grain boundaries and quantifying the stress at failure σ_f. Dugdale et al. [7] delivered the first quantification of the stress at failure ($\sigma_f = 1.35$ GPa) of Alloy 600 grain boundary oxidized under simulated PWR primary coolant conditions, using microcantilevers, whilst Fujii et al. [6] made use of a micro-tensile test strategy and obtained stress at failure values ≤300 MPa. Stratulat et al. [8] reported fracture toughness values from 0.74 to 1.83 MPa $m^{1/2}$ and found that grain boundary character has no comprehensive influence on the values. In this study we show the importance of considering the presence of a surface oxide layer when studying mechanical failure modes via small-scale micromechanical tests, which has been neglected in previous work [7].

2. Experimental aspects

The sample used in this study was provided and oxidized by Institute of Nuclear Safety System (INSS) (Japan) and is the same mill-annealed (30 min at 1050 °C) Alloy 600 coupon used in [7]. The chemical composition is 74.03 wt% Ni, 16.21 wt% Cr, 8.57 wt% Fe, 0.017 wt% C and 0.32 wt% Mn, with some minor impurities of copper, nitrogen, sulphur and silicon. The coupon was exposed to a simulated PWR primary water environment (dissolved hydrogen 30 cm^3/kg, 500 ppm B, 2 ppm Li) at 340 °C for 2000 h. To further accelerate inter-granular (IG) oxide penetration, exposure of the coupon was performed under applied torsion. Thereby each end of the tensile coupon was twisted 20° in opposing directions using a special jig designed by INSS. This

* Corresponding author.
E-mail address: judith.dohr@materials.ox.ac.uk (J. Dohr).

http://dx.doi.org/10.1016/j.tsf.2017.03.060
0040-6090/

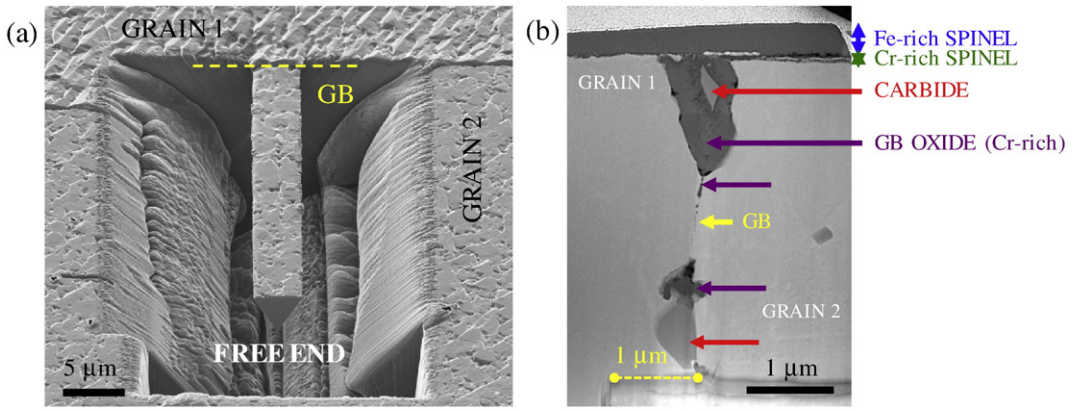

Fig. 1. (a) SEM secondary electron (SE) image of the triangular microcantilever layout with a typical length of ~28 µm and width of ~3.8 µm. A single grain boundary (GB) is included ~1 µm away from the fixed end (yellow line). (b) HAADF scanning TEM image (Jeol ARM200f) of a cantilever cross-section (cantilever 1A) after testing, showing the oxidized surface, preferential grain boundary oxidation, intergranular carbide precipitation and the distance of ~1 µm from the fixed end (yellow line).

resulted in the oxidation of the sample surface, which varied in thickness, morphology and density across the grains (Fig. 1a) and needed to be considered individually, and IG oxidation with reported penetration depths of up to 5 µm (Fig. 1b). The grain diameter was averaged to be approximately 67 µm. The mechanical testing of microcantilevers, prepared with a focused ion beam (FIB), is based on the work by Di Maio [9]. In our study FIB-machined microcantilevers with a triangular cross-section, undercut at 30°, with typical dimensions of 28 µm length and 3.8 µm width (Fig. 1a), were prepared using the method described by [10]. In order to understand the influence of the thin external surface oxide layer on our measurements, two pairs of cantilevers (4 cantilevers in total), each on two different grain boundaries, designated A and B were prepared.

It is known that oxidation along high angle grain boundaries (HABs) reaches significant depths and hence they are most affected by SCC related failure. The grain boundaries tested in this study were high angle grain boundaries (HABs), the misorientation of both grains was calculated based on their specific Euler angles (as measured using Transmission Kikuchi Diffraction) and was shown to be very similar. Whilst Euler angles and corresponding misorientations are given in Table 1, reference axes and are seen in Fig. 4.

In each pair of cantilevers, one cantilever had the surface oxide above the oxidized grain boundary region removed via careful FIB-milling normal to the surface at low beam currents of 10–20 pA at 30 kV. The surface oxide removal was monitored using the SEM (scanning electron microscope) during milling and milling stopped once the oxide layer was removed and the underlying material exposed. Examples of beams after surface oxide removal are shown in Fig. 2, cantilever 2A and 2B. All 4 cantilevers were then tested and the results are summarized in Table 2. Each cantilever included one oxidized grain boundary, approximately 1 µm away from the fixed end where the stress is high, as highlighted by the dashed yellow lines in Fig. 1a and b. Thereby care was taken that the included grain boundary runs as perpendicular to the sample surface as possible.

Table 1
Euler angles (φ_1, ϕ, φ_2) of the fixed end (G_{fixed}, Fig. 4) and free end grain (G_{free}, Fig. 4) for grain boundaries A and B in Bunge notation and corresponding misorientation angles (MA).

Grain boundary	(φ_1, ϕ, φ_2) in (°)		MA in (°)
	G_{fixed}	G_{free}	
A	(4, 28, 313)	(300, 44, 48)	55.7
B	(356, 41, 346)	(242, 26, 147)	55.9

The surface scanning function of a nanoindenter (Agilent NanoIndenter G200) was used to scan the beams prior to testing in order to accurately place a Berkovitch tip onto the free end of the cantilever, which was then used to displace the cantilever at a constant displacement rate of 5 nm/s, and load-displacement data were recorded. After testing, cantilevers were examined in a scanning electron microscope (SEM) (Fig. 2). The load-displacement data and simple beam theory calculations of the beam were then used to perform stress-strain (σ-ε) analysis and to calculate elastic modulus E (Eq. (1)) and stress at failure σ_f (Eq. (2)) of the beams [9,10], as shown in Table 2.

$$E = \frac{\sigma}{\varepsilon}, \text{ with } \varepsilon = \frac{h\delta}{L^2} \tag{1}$$

$$\sigma = \frac{12FL}{wh^2} \tag{2}$$

w is the width, L the length and h the height of the triangular cantilever and F the force and δ the displacement provided by the nanoindenter test.

The moduli obtained for the 4 tested cantilevers (see Table 2) were lower than the average modulus of

207 GPa for A600, as found in literature [11]. However, a comparison with orientation dependent data for single crystal Ni-based super alloys, ~290–320 GPa in ⟨111⟩, ~115–130 GPa in ⟨001⟩ and ~210–230 GPa in ⟨011⟩ direction, shows that the obtained moduli are within a reasonable range [12,13].

Finite element simulations were performed using Abaqus (v6.14) and cohesive surface interaction with a linear traction separation law as described in more detail in [14,15]. The interface is initially elastic until a certain opening displacement, Δ_0, at which point damage initiates and further opening of the interface causes softening until total failure of the interface at Δ_f. In compression the original undamaged stiffness is always used to prevent penetration of the surfaces. The beam dimensions were used to build the geometry of the beams. To obtain realistic but computationally feasible representations of the real cantilever structures along the grain boundaries, the geometry of the beams were extracted using SEM images from the central grain boundary portion of the beam. For reasons of simplicity the 2D sketch of the grain boundary structure generated using the algorithm in [16] was then extruded. Linear hexahedral elements were used with an elastic material law. Extensive mesh convergence studies were performed for all models described in this study to ensure accurate results.